

1  
2  
3  
4 **Characteristics of vertical velocities estimated from drop size and fall**  
5 **velocity spectra of a Parsivel disdrometer**  
6  
7

8 Dong-Kyun Kim and Chang-Keun Song  
9

10 *School of Urban and Environmental Engineering,*  
11 *Ulsan National Institute of Science and Technology, Ulsan, Korea*  
12  
13  
14  
15  
16  
17  
18  
19

20 Submitted to Atmospheric Measurement Techniques  
21  
22  
23  
24  
25  
26

27 Revised on 10 June 2018  
28  
29  
30  
31  
32  
33  
34  
35  
36  
37  
38

---

39 Corresponding Author: Prof. Chang-Keun Song, School of Urban and Environmental Engineering, Ulsan National  
40 Institute of Science and Technology, Ulsan, Korea, Email:cksong@unist.ac.kr

## Abstract

Vertical air velocities were estimated from drop size and fall velocity spectra observed by Parsivel disdrometers during intensive field observations from 13 June to 3 August 2016 around Mt. Jiri (1915 m above sea level) in the southern Korean Peninsula. Rainfall and wind velocity data measured by Parsivel disdrometers and ultrasonic anemometers, respectively, were analyzed for an orographic rainfall event associated with a stationary front over Mt. Jiri on 1 July 2016. In this study, a new technique was developed to estimate vertical air velocities from drop size and fall velocity spectra measured by the Parsivel disdrometers and investigate characteristics of up-/downdrafts and related microphysics in the windward and leeward side of the mountain.

To validate results from this technique, vertical air velocities between the Parsivel disdrometers and anemometers were compared and were shown in quite good agreement each other. It was shown that upward motions were relatively more dominant in the windward side and even during periods of heavy rainfall. On the contrast, downward motions were more dominant in the leeward side during nearly the same periods of heavy rainfall. Occurrences of upward and downward motions were digitized as percentage values as they are divided by a total count of occurrences during the entire period. In the windward (leeward) side, the percentages of upward (downward) motion were much larger than those of downward (upward) motion. The mean rainfall intensity in the leeward side was stronger than in the windward side, suggesting that a large part of rainfall in the leeward side was relatively more affected by the downward motions.

Key words: vertical air velocity, drop size spectra, microphysics, Parsivel disdrometer

## 1. Introduction

Drop size distribution (DSD) and related rain parameters from surface disdrometer measurements or indirectly retrieved from remote sensing measurements such as radars, wind profilers, or satellites provides key information for a better understanding of microphysical processes that account for drop growth or decay within precipitating systems. However, DSD uncertainties always exist as its retrieval is vulnerable to various factors such as measurement errors, sampling difference in volume and height, strong winds, up-/downdrafts, turbulence, and so on as have been reported in many previous studies (Jameson and Kostinski 1998; Cao et al., 2008; Tokay et al., 2009; Thurai et al., 2012). Thus a validation of such retrieved DSDs by comparing with those from surface disdrometers is not straightforward (Williams et al. 2000) due to their different environment although minimizing a sampling difference as much as possible is needed. Even if DSDs are accurately obtained, their characteristics, particularly between convective and stratiform rain, can vary largely from small areas in short-time scale to climatic regimes in long-term.

Ground-based classifications of convective, mixed, or stratiform rain type have been performed in various ways such as characteristics in integral DSD parameters (i.e., rain rate, mean drop diameter, etc), bright band signature, vertical gradients in Doppler velocity and reflectivity, vertical draft magnitude, and so on (Atlas et al., 2000; Cifelli et al., 2000; Thompson et al., 2015; Tokay and Short 1996; Tokay et al., 1996, 1999; Thurai et al., 2016; Williams et al., 1995). Tokay et al. (1999) classified rainfall types from collocated disdrometer and 915 MHz profiler observations in tropical rain events and indicated that compared to profiler classifications that utilize vertical gradients in Doppler velocity, a disdrometer is relatively more feasible to misclassify stratiform rain as convective or vice versa due to time-height ambiguity mostly associated with advection of drops while falling to the ground.

In measuring and validating surface DSDs, there is no such handy, transportable, and low-cost instrument like disdrometer that has long been used as a ground truth although it has inherent problems mentioned above as exposed to all different environments. Parsivel disdrometer (hereafter Parsivel) is one of disdrometers widely used for DSD studies over the world. As deduced from its name, par-si-vel (particle size and velocity), this disdrometer measures fall velocities, sizes, and number counts of liquid and ice particles falling into 32 (size) x 32 (fall velocity) bins. Parsivel has been used at observatories or in numerous field experiments to examine and validate microphysical properties by comparing DSDs and integral DSD parameters with those from other type disdrometer, 2-Dimensional Video Disdrometer (2DVD) and radar and profiler observations for various events of precipitation (Jaffrain and Berne 2011; Kim et al., 2016; Thurai et al., 2011, 2016; Tokay et al., 2013).

A Parsivel-measured fall velocity of a raindrop is the sum of a raindrop terminal fall speed (in stagnant air) and vertical air motion. Thus when there are updrafts or downdrafts, the Parsivel-measured fall velocity is deviated from the terminal fall speed even if drop sizes are identical. On top of this, strong horizontal winds, vertical shear, or turbulence can disperse the distribution of drop size and fall velocity, leading to a change (or bias) in the Parsivel-measured fall velocity averaged over the distribution. Consequently, all these factors would affect DSD integral parameters such as rain rate although the effects of the factors on DSD are complicated and hardly discriminated (Niu et al., 2010). Ulbrich (1992) examined errors in rain rate that result from inaccuracies in fall speeds of raindrops (i.e., inaccurate estimation of vertical air motion) and indicated that updraft will result in larger rain rate at a given reflectivity than when there are no vertical winds. Niu et al. (2010) investigated differences in distributions of drop sizes and fall velocities between convective and stratiform rain and ascribed different deviations in Parsivel-measured fall velocities between small and large drops to vertical air motion and turbulence. Parsivel is prone to measurement errors

particularly when there are strong winds and turbulence, leading to discrepancies in comparison with other measurements in the same locations. Friedrich et al. (2013) investigated the influence of strong winds on particle size distributions measured by Parsivel disdrometers deployed in Hurricane Ike 2008 and convective storms and noted that misclassification can occur by particles not falling perpendicular to the sampling area at high wind speed and/or heavy rainfall. Tokay et al. (2009, 2014) indicated that the old version of Parsivel tends to underestimate the number of small drops and overestimate drop size larger than 2.0 mm in heavy rain as well as in windy conditions. When they compared each old and new version of Parsivel with Joss-Waldvogel disdrometer and rain gauge measurements, the new version of Parsivel (referred to as Parsivel<sup>2</sup> in their paper) appeared to have a noticeable improvement over the old one for measuring drop size and rainfall rate.

To our knowledge, no studies of vertical air velocities retrieved from Parsivel-measured drop size-fall velocity spectra have been documented or reported yet. In this study we utilize Parsivel and anemometer data collected during intensive field observations that targeted to investigate orographic rainfall mechanisms around mountain areas in the southern region of Korea. A simple technique to retrieve vertical air velocities from Parsivel measurements is developed and first applied to an orographic heavy rain event. This paper is organized as follows. In Section 2, the retrieval technique and instruments used in this study are introduced. A case description about the rain event is followed in Section 3. Results about characteristics of up-/downward motions and related microphysics in the windward and leeward side are presented in Section 4. A summary and conclusions follow in Section 5.

## **2. Instrumentation and method**

Two main instruments used in this study are Parsivel disdrometer and ultrasonic anemometer collocated at three different sites around Mt. Jiri (see Figure 1). Their data were

collected during the intensive observation period from 13 June to 3 August 2016 to cover a summer rainy season which is called “Changma” in Korea were analyzed. Parsivel disdrometer (Parsivel), manufactured by OTT (Germany), uses laser-optical properties to measure both sizes and fall velocities of precipitation particles and derives quantities of radar reflectivity, precipitation intensity, etc from measured drop spectra. Time resolution is 1 min. For more details about Parsivel, please see the Löffler-Mang and Joss (2000)’s paper. The ultrasonic anemometer (the Young Model 81000, hereafter UVW) measures east-west ( $u$ ), north-south ( $v$ ), and vertical ( $w$ ) components of winds by using the speed of sound moving along winds between the three non-orthogonal sonic axes and generates wind speed and direction at 1-min interval. The accuracies are  $\pm 0.05 \text{ m s}^{-1}$  for wind speed (0 to  $30 \text{ m s}^{-1}$ ) and  $\pm 2$  degrees for wind direction (0 to  $30 \text{ m s}^{-1}$ ), respectively. The  $w$  component observed by UVW is referred to as  $w_{UVW}$ .

In this study, a simple, new scheme to derive vertical air velocity ( $w$ ) from Parsivel measurements is developed by using a relationship of Atlas et al. (1973) between terminal fall velocities and drop diameters in still air as shown by

$$V_f = 9.65 - 10.43 \cdot \exp(-0.6D), \quad (1)$$

where  $D$  is drop diameter (mm) and  $V_f$  is terminal fall velocity ( $\text{m s}^{-1}$ ) and also the vertical relation of air as shown below

$$w = V_p - V_f, \quad (2)$$

where  $V_p$  is Parsivel-measured fall velocity ( $\text{m s}^{-1}$ ) averaged over 32 diameter x 32 velocity classes in a size and velocity spectrum. Altitudes of D1, D2, and D4 are 105, 280 and 313 m ASL, respectively. Due to the very low altitudes of these observation sites, change in atmospheric density with height is negligible and thus the atmospheric density correction

(Beard, 1985) on  $V_f$  is ignored. In all the terms, negative means downward. A mean  $w$  value at 1-min interval is finally estimated by subtracting  $V_p$  from  $V_f$  also averaged following the flowchart in Figure 2. The final  $w$  estimate is hereafter called  $w_{par}$ . For more details, please see the flowchart that shows how  $w$  is estimated from a 1-min drop size ( $D$ ) and fall velocity ( $V_p$ ) spectrum of Parsivel. Figure 3 illustrates three conditions of determining zero  $w$ , upward  $w$ , or downward  $w$  value for given  $D$  vs.  $V_p$  spectra. For the case 1,  $w$  would be zero since the  $D$ - $V_p$  distribution closely follows the  $V_f$  line. Upward  $w$  value is determined for the case 2 that  $V_p$  is smaller than  $V_f$  (i.e., the distribution is towards below the  $V_f$  line). For the case 3, downward  $w$  value is determined since  $V_p$  is larger than  $V_f$ . For  $w_{par}$  validation,  $w_{par}$  is compared with  $w_{UVW}$  and its result is described in Section 4.

### 3. Case description

During a summer rainy season usually from late June to mid July in Korea, severe weather phenomena accompanied by heavy rainfall often occur in the southern region of the Korean Peninsula mostly covered by complex high mountains. In association with terrain-induced up-/downdrafts, mountainous areas can play an important role in controlling formation, amount, and distribution of rainfall. As precipitation systems move over these areas, they tend to develop rapidly and produce localized heavy rainfall. Observational analysis from radar and surface measurements in these areas is necessary to understand terrain effects on rainfall development and microphysics. Thus we performed intensive field observations around Mt. Jiri (1915 m ASL) in the southern Korean Peninsula during the 2016 summertime.

During the observation period of 13 June~3 August 2016, several rain events were observed. On 1 July 2016, a rainfall system associated with a Changma front has developed over the West Sea and moved towards Mt. Jiri. As it passes over the mountain from the east,

heavy rainfall was produced and observed by Parsivel disdrometers and UVWs from 1200 to 2200 UTC. Figure 4 shows a distribution of accumulated rainfall on 1 July and the enlarged topography of Mt. Jiri with locations of observations. Large rainfall up to 90 mm was seen around the top and south of Mt. Jiri in relation to moist upwind flows in the windward side close to the ocean.

## 4. Results

### 4.1. $w$ comparison in time series

For the  $w_{par}$  validation, the observed  $w_{UVW}$  is compared at time series. Time series of radar reflectivity ( $Z$ ), rain rate ( $R$ ), mass-weighted mean diameter ( $D_m$ ) measured from Parsivel are also examined together. Three observation sites of D1, D2, and D4 where both the Parsivel and UVW data are available were selected out of total nine sites (Fig. 4b). D1 and D2 are windward and D4 is leeward of Mt. Jiri. Figure 5 shows the time series of  $Z$ ,  $R$ , and  $D_m$  (top) and  $w$  (bottom) between the Parsivel and UVW observed at D1, D2, and D4. At D1 and D2, high  $Z > 40$  dBZ and  $R > 20$  mm h<sup>-1</sup> are observed during the 1230-1330 UTC period and around 1730 UTC in Figs. 5a and c. Correspondingly, large  $D_m$  values reaching 2 mm were analyzed in these periods. In Fig. 5e, high  $Z$  and  $R$  were also observed in the leeward side but showing a little time lag compared to those in Figs. 5a and c.

It is shown in Figs. 5b, d, and f that  $w_{par}$  matches quite well with  $w_{UVW}$ . On the windward side (D1, D2), they both show mostly upward motions and importantly, larger upward motions during periods of heavy rainfall (i.e., 1230-1330 UTC and around 1730 UTC). In contrast, downward motions are mostly observed on the leeward side (D4). It is noted in Fig. 5f that there existed relatively large difference between  $w_{par}$  and  $w_{UVW}$  during these high  $R$  periods. We found that the difference is related to a decrease of  $V_p$  in these periods. For a given  $V_f$ , a mean  $V_p$  became smaller in Eq (2) due to an increase of a larger number of small



drops ranged at 1~2 mm or a spread of small drops below the  $V_f$  line in the  $D$ - $V_p$  distribution, more like the case 2 illustrated in Fig. 3. A physical reason for this is not clear yet but it is probably resulted from strong winds and turbulence during this high  $R$  periods. In other periods, they showed quite good agreement. Also, the maximum and minimum values of  $w_{par}$  and  $w_{UVW}$  hardly exceed  $\pm 0.5 \text{ m}^{-1}$ , almost the one fifth of horizontal wind magnitudes (not shown), suggesting that winds are almost horizontal during the whole period and they point upward or downward slightly with the  $w$  signs. At D1 and D2, the relatively large  $w_{par}$  and  $w_{UVW}$  were found during heavy rain with  $R > 20 \text{ mm h}^{-1}$  around 1300 and 1740 UTC (Figs. 5b and d), indicating that updrafts contributed more on the substantial  $R$  increase on the windward side. In Fig. 5f, negative  $w_{UVW}$  values were found on the leeward side most of the time including the heavy rain period ( $R > 20 \text{ mm h}^{-1}$ ), suggesting that most of rainfall on the leeward side occurred in more association with downward  $w$  motions.

Figure 6 shows characteristics of  $Z$ - $R$  relations at D1, D2, and D4. Upward  $w_{par}$  values are colored in red and downward  $w_{par}$  in blue. They were changed to percentages by dividing by a total of counts in each class with  $R > 0.5 \text{ mm h}^{-1}$ . At D1 and D2, the percentage for the upward  $w_{par}$  class is 61% and 71%, much larger than 39% and 29% for the downward  $w_{par}$  class, respectively. In contrast, the upward  $w_{par}$  percentage at D4 is 31%, about a half or less than those at D1 and D2 as found in Fig. 5, and the downward  $w_{par}$  percentage is 69%. Power-law  $Z$ - $R$  relations in a form of  $Z = \alpha R^\beta$  are compared between the observation sites in Fig. 6. There was a decrease in the coefficient  $\alpha$  from D1 and D2 (250, 252) on the windward side to D4 (226) on the leeward side. The exponent  $\beta$  did not show notable change between the sides. The noticeable decrease in  $\alpha$  suggests that for a given  $Z$ ,  $R$  is larger at D4 than D1 and D2. This is consistent to histograms of DSD parameters in the later section showing the larger mean  $R$  and  $D_m$  at D4.

## 4.2. Histogram analyses

### 4.2.1 Characteristics of $w$ histograms with regard to $R$

The  $w_{par}$  and  $w_{UVW}$  time series discussed in Section 4.1 are examined in their histograms of frequency with regard to  $R$ . In this study, a simple  $R$  threshold,  $R < 10 \text{ mm h}^{-1}$  and  $R > 10 \text{ mm h}^{-1}$  (Leary and Houze 1979; Testud et al., 2001), to discriminate stratiform and convective rain was used although there have been a plenty of other methods based on DSDs and vertical profiles to discriminate stratiform and convective rain (Bringi et al., 2003; Caracciolo et al., 2006; Thompson et al., 2015; Thurai et al., 2016; Tokay and Short 1996; Tokay et al., 1999; Ulbrich and Atlas 2002; Williams et al., 1995). Occurrences of upward and downward motions were changed to percentage values as they are divided by a total count of upward and downward  $w$  during the entire period. A bin size for these histograms is  $0.05 \text{ m s}^{-1}$ .

In Figs. 7a, b, c, on the whole, the  $w_{par}$  histograms are in good agreement with the  $w_{UVW}$  at all three sites, showing the much better agreement in the stratiform class ( $R < 10 \text{ mm h}^{-1}$ ) than the convective class. The relatively larger difference between the  $w_{par}$  and  $w_{UVW}$  histograms is found in the convective class of D1 and this is likely due to strong wind speeds that tend to make a downward spread in measured  $D$  vs.  $V_p$  spectra of Parsivel. Mathematically, this downward spread decreases Parsivel-measured drop fall velocities (i.e., decrease in  $V_p$  in Eq (2)) and hence  $w_{par}$  becomes more positive, making a larger difference with  $w_{UVW}$ . Compared to D4, the similar histograms of  $w_{par}$  are shown between D1 and D2. That is, convective rain has occurred almost in association with upward motions, while for stratiform rain, it occurred with both upward and downward motions (Figs, 7a and b). At D4, in contrast, most of stratiform rain was associated with downward motions and convective rain was associated with both upward and downward motions (Fig. 7c). Therefore, both convective and stratiform rain was relatively more associated with downward motions on the

leeward side than on the windward side. Figures 7d,e,f show the areas occupied by the upward and downward  $w$  motions in percentage at each site, same as those in the  $Z$ - $R$  scatterplots shown in Fig. 6. The colored areas with the percentages show readily which  $w$  group is far dominant. As noted, upward motions were dominant at D1 and D2 while downward motions were dominant at D4. However, they did not show large percentage differences at all the sites, suggesting that either upward or downward motions have not happened overwhelmingly in this event.

#### 4.2.2 Characteristics of $Z$ histograms with regard to $w$ and $R$

The  $w_{par}$  properties discussed in Section 4.1 are examined by frequency histograms of  $Z$  with regard to  $w$  and  $R$ . In Fig. 8a, a much larger percentage (61%) in the upward  $w$  group is found at D1 showing a relatively wider  $Z$  distribution, compared to that at D4 in Fig. 8d. In Fig. 8b, the  $R$  percentage classified as convective was 9%, much smaller than 61% in the upward  $w$  group in Fig. 8a, suggesting that 52% of the upward  $w$  group was associated with stratiform rain. In order to study such relationships between  $w$  and  $R$ , histograms were split by four conditions in the upper-right corner shown in Figs. 8c and f. That is, each group of  $R > 10 \text{ mm h}^{-1}$  and  $R < 10 \text{ mm hr}^{-1}$ , which is regarded as convective and stratiform rain, respectively, is separated by upward and downward  $w$ . Therefore, for instance, 91% of the group  $R > 10 \text{ mm h}^{-1}$  in Fig. 8c is equal to the sum of 52% of the upward  $w$  and 39% of the downward  $w$  group. Likewise, the upward and downward  $w$  group is also split by the two  $R$  conditions. Unlike D4 in Fig. 8f, there was no thick blue line at D1 in Fig. 8c because there were no data fell into this category of the downward  $w$  and  $R > 10 \text{ mm h}^{-1}$  as shown in Fig. 7a.

In Fig. 8c, convective rain ( $R > 10 \text{ mm h}^{-1}$ ) with the largest mean  $Z$  has occurred solely in association with upward  $w$  motions (thick red line). Among the four categories, the majority percentage of 52% was found in the category of the upward  $w$  and  $R < 10 \text{ mm h}^{-1}$  at D1 but

65% was found in the category of the downward  $w$  and  $R < 10 \text{ mm h}^{-1}$  at D4. The widest  $Z$  distribution were shown in these categories. In Fig. 8d, a much larger percentage is found in the downward  $w$  group as noted previously. In Fig. 8e, a larger percentage of 18% is found in the group  $R > 10 \text{ mm h}^{-1}$ , compared to the counterpart (9%) at D1, indicating that on average sense, rain intensity was stronger at D4 (leeward). It is noted that at D4, convective rain has occurred in association with both upward (14%) and downward motions (4%) although the latter showed a bit smaller  $Z$  values than those in the upward  $w$ -convective rain category (thick red line). It is thus suggested that downward  $w$  motion can play a significant role in increasing  $R$ , even larger than  $10 \text{ mm h}^{-1}$  although the strongest  $R$  was related to upward motions rather than downward. Most of stratiform rain was associated with downward motions (65%).

#### 4.2.3. Histogram characteristics of DSD parameters with regard to $w_{par}$

In Fig. 9, we analyze histograms of DSD parameters that are obtained with additional  $w$  information from Parsivel, which is a first time ever, compared to conventional DSD studies. In this study, two histograms separated by the upward and downward  $w$  were obtained *per* each parameter. In Fig. 9b, The  $Z$  histograms at D4 show higher  $Z$  distributions with mean values of 34.8 and 25.6 dBZ in the upward and downward  $w$  category, respectively, are shown, compared to those (25.2 and 18.2 dBZ) at D1 in Fig. 9a. At both D1 and D4, the mean  $Z$ ,  $R$ , and  $D_m$  values in the upward  $w$  category were higher than those in the downward  $w$  category. Between D1 and D4, the mean  $Z$ ,  $R$ , and  $D_m$  over the entire data were higher at D4, indicating that rainfall intensity was somewhat stronger than D1 although the maximum  $Z$  ( $\sim 50 \text{ dBZ}$ ) and  $R$  (near  $60 \text{ mm hr}^{-1}$ ) were quite similar each other (see the time series of  $Z$  and  $R$  in Fig. 5). The mean  $R$  of  $15.1 \text{ mm hr}^{-1}$  was higher in the upward  $w$  category of D4 than  $6.22 \text{ mm hr}^{-1}$  in that of D1 (Figs. 9c and g). The total mean  $R$  was  $7.2 \text{ mm hr}^{-1}$  at D4, also

larger than  $4.3 \text{ mm hr}^{-1}$  at D1. The mean  $D_m$  was largest at 1.37 mm in the upward  $w$  category of D4 in Fig. 9f and smallest at 0.86 mm in the downward  $w$  category of D1 in Fig. 9b. Thus, the mean  $D_m$  (1.03 mm) in the downward  $w$  category of D4 was greater than that (0.86 mm) in that of D1. This indicates that there were a comparatively larger number of large drops at D4 in association with downward motions which were dominant during the entire period. Thus, it is stressed that relative to the windward side, downward motions have more influenced the growth in drop size and increase in  $R$  intensity in the leeward side.

## 5. Summary and conclusions

Intensive field observations for orographic rainfall around Mt. Jiri in the southern regions of Korea were conducted during summertime in 2016. In order to examine up-/downward  $w$  properties in the windward and leeward side of the mountain, a simple technique was newly developed to retrieve vertical velocities ( $w$ ) from drop size and fall velocity spectra of Parsivel. Their comparison with the  $w$ -components observed by UVW showed quite good agreement each other, producing the similar  $w$  histograms between the two instruments. On the windward side (D1 and D2), upward motions were more frequently observed and particularly larger upward motions were found during convective rain. For the leeward side (D4), downward motions were more dominant even during the large  $R$  periods ( $> 10 \text{ mm hr}^{-1}$ ) as in the windward side. Most of stratiform rain was associated with downward motions. Thus, it is speculated that downward motions have contributed more to drop growth and  $R$  increase in the leeward side. It is important to note that as the rain system moves over the mountain, upward and downward motions have occurred in the both sides of the mountain although there existed differences in their frequencies of occurrence.

Eventually the newly developed technique that estimates  $w$  values from Parsivel drop size and fall velocity spectra is found physically meaningful although it needs to be further tested

in other places and events. It would be applicable to  $w$  retrieval and comparison studies near the surface to investigate rain microphysics associated with up-/downward motions. The different  $w$  percentages in the different locations stressed their dependence on observed  $D-V_p$  distributions which vary largely as a result of complex factors such as rainfall intensity, up-/downdrafts, wind speed, turbulence, and so on.

In this study, both the observed and estimated  $w$  values were very small in magnitude mostly between  $-0.5$  and  $+0.5 \text{ m s}^{-1}$ , about the one fifth of the measured horizontal wind speeds. As known, the  $w$  values are just a vertical component of winds. Thus the low  $w$  values indicate almost horizontal winds that head up and down slightly with the  $w$  signs. During the high  $R$  periods, the estimated  $w$  values were larger in a positive sign (windward side), suggesting that there were slightly upward flows around the mountain. Probably this produces an environment of converging-upward air in large scale and helps to intensify the orographic rain system, increasing  $Z$  and  $R$ .

The relatively large difference between  $w_{par}$  and  $w_{UVW}$  was found in the leeward side during the high  $R$  periods (Fig. 5f). This is probably associated with strong winds and turbulence that may spread the  $D-V_p$  distribution of drops down below the  $V_f$  line and further bias  $w$  magnitudes. Hence the  $w$  retrieval from the disdrometer-based technique is not totally free from environmental conditions. Since the effects of winds and turbulence were not analyzed in this study, we will soon investigate their effects on  $D-V_p$  distributions as well as resultant  $w$  biases in a quantitative way as a subsequent work.

## **Acknowledgements**

This research was supported by the National Strategic Project-Fine Particle of the National Research Foundation of Korea(NRF) funded by the Ministry of Science and ICT(MSIT), the Ministry of Environment(ME), and the Ministry of Health and Welfare(MOHW).(NRF-2017M3D8A1092021)

## References

- Atlas, D., Srivastava, R. C., Sekhon, R. S., 1973. Doppler radar characteristics of precipitation at vertical incidence. *Rev. Geophys. Space Phys.*, 11, 1–35.
- Atlas, D., Ulbrich, C. W., Marks, F. D., Black, R. A., Amitai, E., Willis, P. T., Samsury, C. E., 2000. Partitioning tropical oceanic convective and stratiform rains by draft strength. *J. Geophys. Res.*, 105, 2259–2267.
- Beard, K. V., 1985: Simple altitude adjustments to raindrop velocities for Doppler radar analysis. *J. Atmos. Oceanic Technol.*, 2, 468–471.
- Bringi, V. N., Chandrasekar, V., Hubbert, J., Gorgucci, E., Randeu, W. L., Schoenhuber, M., 2003. Raindrop size distribution in different climatic regimes from disdrometer and dual-polarized radar analysis. *J. Atmos. Sci.* 60, 354–365.
- Cao, Q., Zhang, G., Brandes, E., Schuur, T., Ryzhkov, A., Ikeda, K., 2008. Analysis of Video Disdrometer and Polarimetric Radar Data to Characterize Rain Microphysics in Oklahoma. *J. Appl. Meteor. Climatol.* 47, 2238–2255.
- Caracciolo, C., F. Prodi, A. Battagliac, Porcu, F., 2006. Analysis of the moments and parameters of a gamma DSD to infer precipitation properties: a convective stratiform discrimination algorithm. *Atmos. Res.*, 80, 165–186.
- Cifelli, R., Williams, C. R., Rajopadhyaya, D. K., Avery, S. K., Gage, K. S., May, P. T., 2000. Drop-size distribution characteristics in tropical mesoscale convective systems. *J. Appl. Meteor.* 39, 760–777.
- Friedrich, K., S. Higgins, F. J. Masters, and C. R. Lopez, 2013b: Articulating and stationary Parsivel disdrometer measurements in conditions with strong winds and heavy rainfall. *J. Atmos. Oceanic Technol.*, **30**, 2063–2080.
- Jaffrain, J., and A. Berne, 2011: Experimental quantification of the sampling uncertainty associated with measurements from PARSIVEL disdrometers. *J. Hydrometeorol.*, 12,



352–370.

Jameson AR, Kostinski AB. 1998. Fluctuation properties of precipitation. Part II: reconsideration of the meaning and measurement of raindrop size distributions. *J. Atmos. Sci.* 55: 283–294.

Kim, D.-K., and D.-I. Lee, 2016: Raindrop size distribution properties associated with vertical air motion in the stratiform region of a springtime rain event from 1290-MHz wind profiler, micro rain radar, and Parsivel disdrometer measurements, *Meteorological Applications*, 23, 40-49.

Leary, C. A., and R. A. Houze Jr., 1979: Melting and evaporation of hydrometeors in precipitation from the anvil clouds of deep tropical convection. *J. Atmos. Sci.*, 36, 669–679.

Löffler-Mang, M., and J. Joss, 2000: An optical disdrometer for measuring size and velocity of hydrometeors. *J. Atmos. Oceanic Technol.*, 17, 130–139.

Niu, S., X. Jia, J. Sang, X. Liu, C. Lu, and Y. Liu, 2010: Distributions of raindrop sizes and fall velocities in a semiarid plateau climate: Convective versus stratiform rains. *J. Appl. Meteor. Climatol.*, 49, 632–645.

Testud, J., S. Oury, P. Amayenc, and R. A. Black, 2001: The concept of “normalized” distributions to describe raindrop spectra: A tool for cloud physics and cloud remote sensing. *J. Appl. Meteor.*, 40, 1118–1140.

Thompson, E. J., S. A. Rutledge, B. Dolan, and M. Thurai, 2015: Drop size distributions and radar observations of convective and stratiform rain over the equatorial Indian and west Pacific Oceans. *J. Atmos. Sci.*, **72**, 4091–4125.

Tokay, A., Short, D. A., 1996. Evidence from Tropical raindrop spectra of the origin of rain from stratiform versus convective clouds. *J. Appl. Meteor.* 35, 355–371.

Tokay, A., Short, D. A., Williams, C. R., Ecklund, W. L., Gage, K. S., 1999. Tropical rainfall

associated with convective and stratiform clouds: Intercomparison of disdrometer and profiler measurements. *J. Appl. Meteor.* 38, 302–320.

Tokay A, Hartmann P, Battaglia A, Gage KS, Clark WL, Williams CR. 2009. A field study of reflectivity and Z–R relations using vertically pointing radars and disdrometers. *J. Atmos. Oceanic Technol.* 26: 1120–1134.

Tokay, A., W. A. Petersen, P. Gatlin, and M. Wingo, 2013: Comparison of raindrop size distribution measurements by collocated disdrometers. *J. Atmos. Oceanic Technol.*, **30**, 1672–1690.

Tokay, A., Wolff, D. B., Petersen, W. A., 2014. Evaluation of the new version of the laser-optical disdrometer, OTT Parsivel<sup>2</sup>. *J. Atmos. Oceanic Technol.* 31, 1276–1288.

Thurai, M., W. A. Petersen, A. Tokay, C. Schultz, and P. Gatlin, 2011: Drop size distribution comparisons between Parsivel and 2D video disdrometers. *Adv. Geosci.*, **30**, 3–9.

Thurai M, Bringi VN, Carey LD, Gatlin P, Schultz E, Petersen WA. 2012. Estimating the accuracy of polarimetric radar–based retrievals of drop-size distribution parameters and rain rate: an application of error variance separation using radar-derived spatial correlations. *J. Hydrometeor.* 13: 1066–1079.

Thurai, M., Gatlin, P. N., Bringi, V. N., 2016. Separating stratiform and convective rain types based on the drop size distribution characteristics using 2D video disdrometer data. *Atmos. Res.*, 169, 416–423.

Ulbrich, C.W., 1992. Algorithms for determination of rainfall integral parameters using reflectivity factor and mean doppler fall speed at vertical incidence. *J. Atmos. Ocean. Technol.* 9, 120–128.

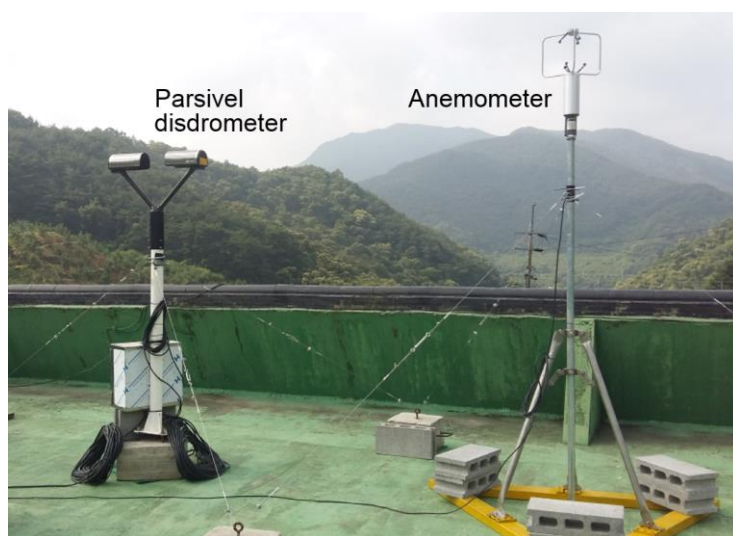
Ulbrich, C. W., and D. Atlas, 2002: On the separation of tropical convective and stratiform rains. *J. Appl. Meteor. Climatol.*, 41, 188–195.

Williams, C. R., Ecklund, W. L., Gage. K. S., 1995. Classification of precipitating clouds in

the tropics using 915-MHz wind profilers. *J. Atmos. Oceanic Technol.*, 12, 996-1012.

Williams, C. R., A. Kruger, K. S. Gage, A. Tokay, R. C. Cifelli, W. F. Krajewski, and C. Kummerow, 2000: Comparison of simultaneous rain drop size distributions estimated from two surface disdrometers and a UHF profiler. *Geophys. Res. Lett.*, 27, 1763–1766.

508  
509  
510  
511  
512  
513  
514  
515  
516  
517  
518  
519  
520  
521  
522



523  
524  
525  
526  
527  
528  
529  
530  
531  
532  
533  
534  
535  
536  
537  
538  
539  
540  
541  
542  
543  
544  
545

Figure 1. Picture of a Parsivel disdrometer and 3-D anemometer that were installed at an observation site around Mt. Jiri during the intensive observation period.

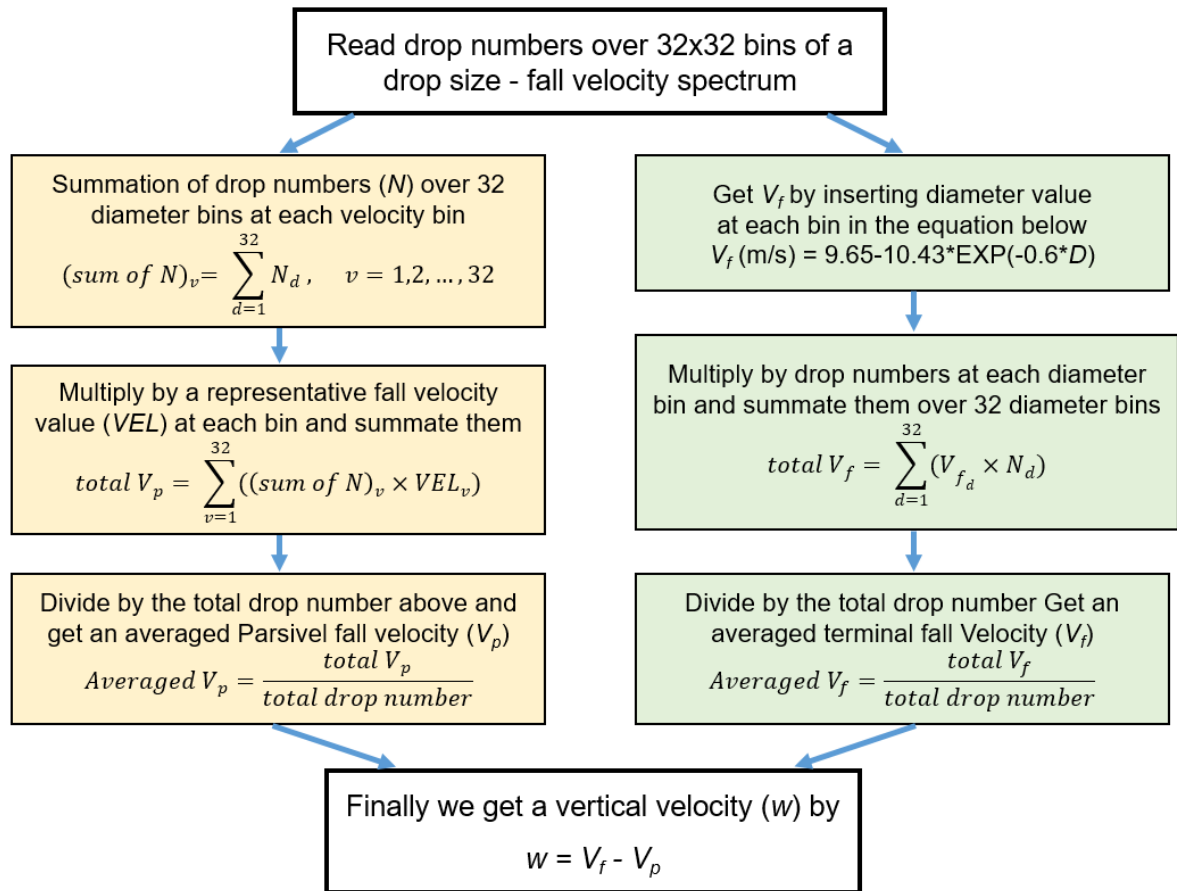
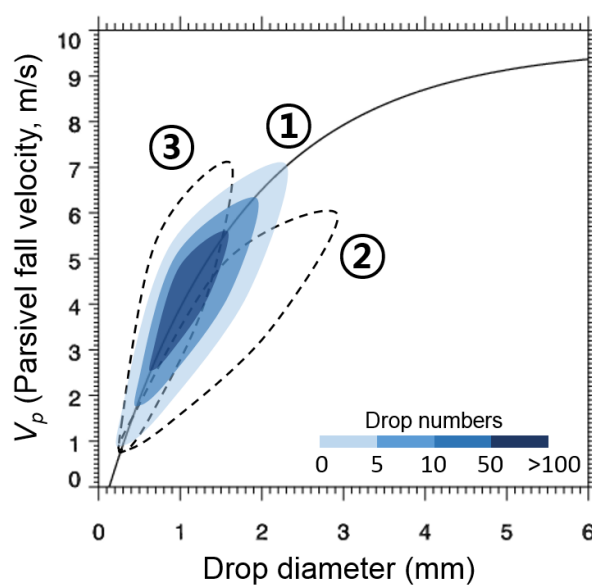


Figure 2. Flowchart for estimating  $w$  from a diameter-fall velocity spectrum of Parsivel (1-min interval). See text for more details.

573  
574  
575  
576  
577  
578  
579  
580  
581  
582  
583  
584  
585  
586



587  
588  
589  
590  
591  
592  
593  
594  
595  
596  
597  
598  
599  
600  
601  
602  
603  
604  
605  
606  
607  
608

Figure 3. Schematic of Parsivel-observed diameter and fall velocity distributions for the three cases of determining zero  $w$ , upward  $w$ , and downward  $w$ . Contours show drop number concentrations. See text for more information.

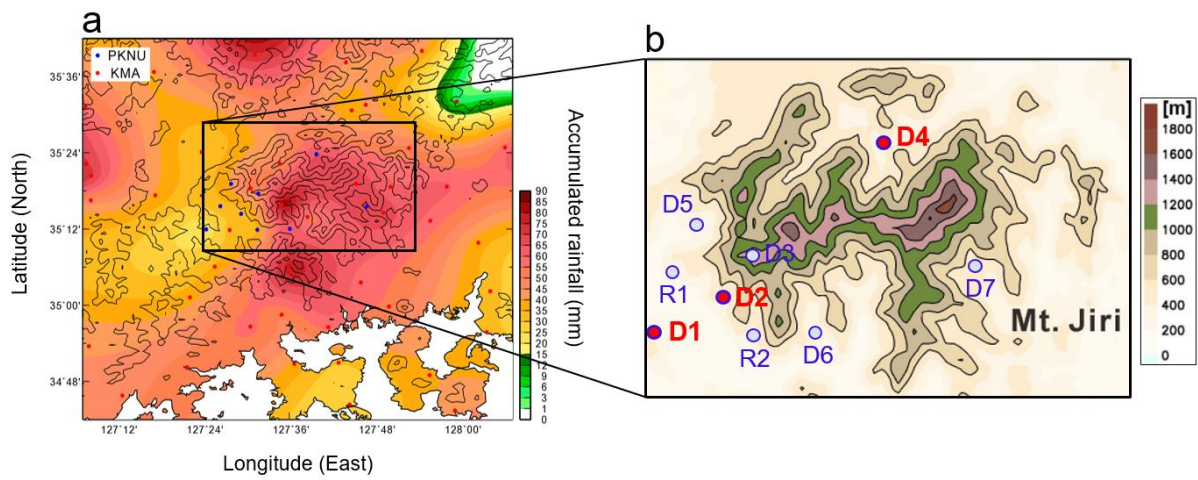


Figure 4. (a) Distribution of an accumulated rainfall (mm) on 1 July over contours of altitude at 300 m interval and (b) the enlarged topography of Mt. Jiri with contours of altitude at 200 m interval, showing nine observation sites. Three sites in red are where the Parsivel and UVW measurements were analyzed in this study. R1 and R2 show sites with a rain gauge only.

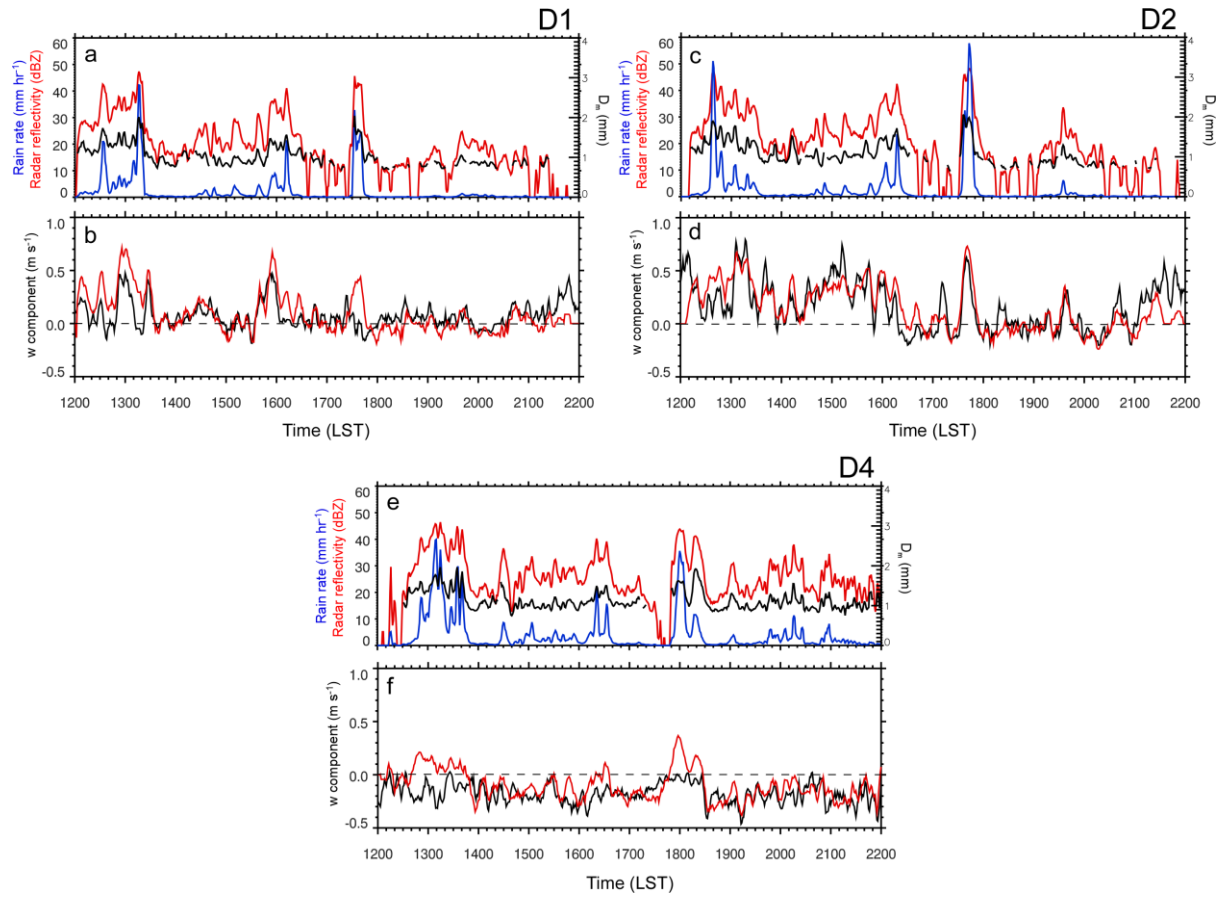


Figure 5. Time series of radar reflectivity (dBZ) in red line, rain rate (mm hr<sup>-1</sup>) in blue, and mass-weighted mean diameter ( $D_m$ , mm) in black at D1, D2, and D4 ((a),(c),(e)) and the time series of  $w_{par}$  (m s<sup>-1</sup>) in red and  $w_{UVW}$  (m s<sup>-1</sup>) in black at the same sites ((b),(d),(f)). 5-point running mean was applied.



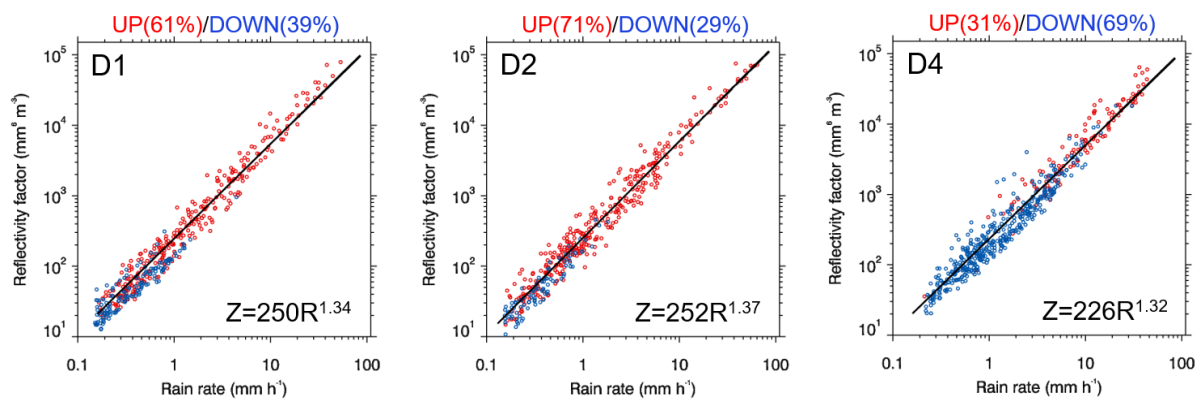


Figure 6. Z-R scatterplots at the three sites. Red dots indicate upward  $w$  and blue indicate downward  $w$ . Numbers on the top show percentages of occurrence frequency in each  $w$  category.

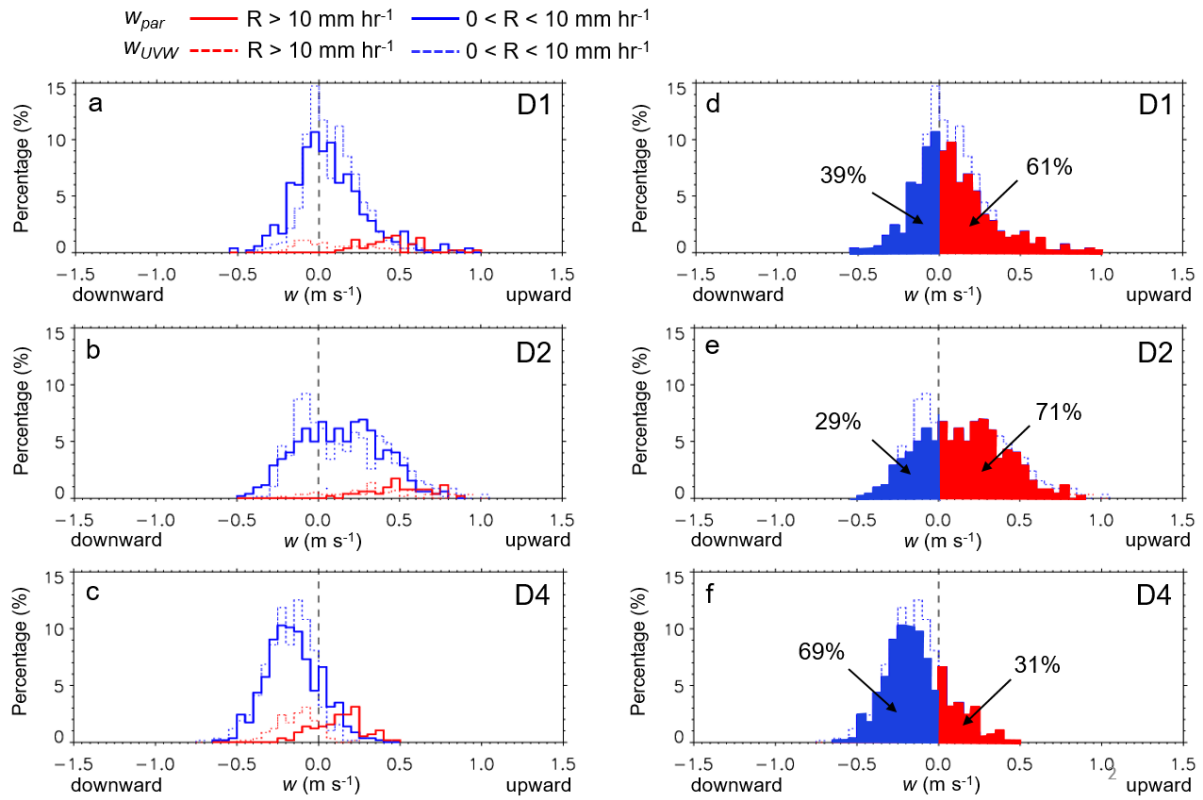


Figure 7. Frequency histograms of  $w$  with regard to the two  $R$  groups (left) and those with percentages in the upward and downward  $w$  groups at the three sites (right).

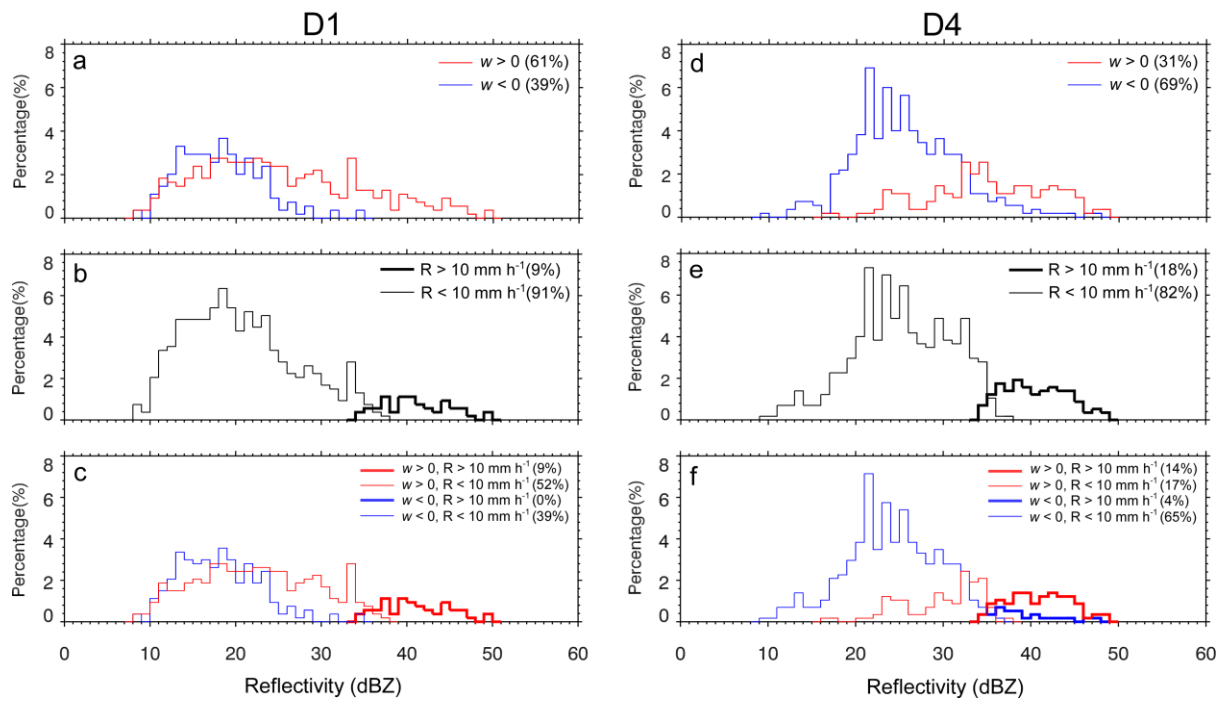


Figure 8. Frequency histograms of  $Z$  with regard to  $w$ ,  $R$ , and those in the four groups with percentage at D1 and D4.

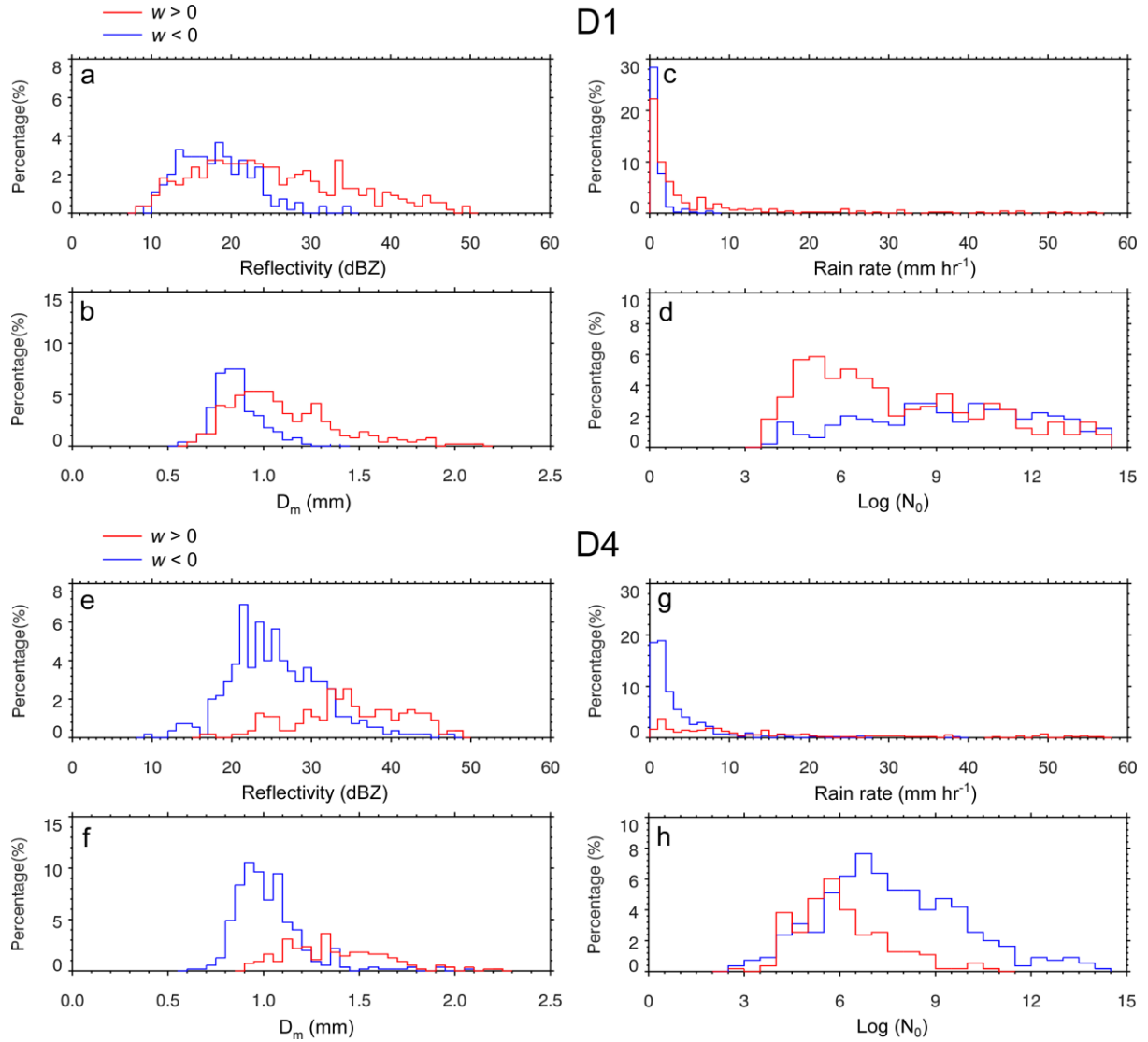


Figure 9. Frequency histograms of retrieved DSD parameters with regard to the upward (red line) and downward  $w$  (blue): (a) radar reflectivity (dBZ), (b) rain rate ( $\text{mm hr}^{-1}$ ), (c)  $D_m$  (mm) and (d)  $N_0$  in log scale at D1 (top four panels) and the same as these but for D4 (bottom four panels).